

Phase separation of bacterial colonies in a limit of high degradation. Analogy with Jupiter's great red spot.

P.H. Chavanis

Laboratoire de Physique Théorique, Université Paul Sabatier, 118 route de Narbonne 31062 Toulouse, France
e-mail: chavanis@irsamc.ups-tlse.fr

To be included later

Abstract. We discuss the structure of the equilibrium states of a regularized Keller-Segel model describing the chemotaxis of bacterial populations. We consider the limit of high degradation of the secreted chemical where analytical results can be obtained. Below a critical effective temperature, the system experiences a second order phase transition from a homogeneous phase to an inhomogeneous phase formed by two domains with uniform concentration separated by a thin interface (domain wall). We study the properties of the interface and determine the bifurcation between a circular shape (spot) and a stripe as a function of the control parameters. We show the analogy with the structure of Jupiter's Great red spot which also consists of two phases with uniform potential vorticity separated by a thin annular jet.

PACS. 05.20.-y Classical statistical mechanics – 05.45.-a Nonlinear dynamics and nonlinear dynamical systems

1 Introduction

The name chemotaxis refers to the motion of organisms induced by chemical signals [1]. In some cases, the biological organisms secrete a substance (pheromone, smell, food, ...) that has an attractive effect on the organisms themselves. Therefore, in addition to their diffusive motion, they move systematically along the gradient of concentration of the chemical they secrete (chemotactic flux). When attraction prevails over diffusion, the chemotaxis can trigger a self-accelerating process until a point at which aggregation takes place. This is the case for the slime mold *Dictyostelium Discoideum* and for the bacteria *Escherichia coli*. A model of slime mold aggregation has been introduced by Patlak [2] and Keller & Segel [3] in the form of two coupled differential equations. A simplified version of this model has been extensively studied in the case where the degradation of the secreted chemical can be neglected. In that case, the Keller-Segel equations become isomorphic to the Smoluchowski-Poisson system describing self-gravitating Brownian particles [4]. An analytical study of this system of equations has been performed by Chavanis & Sire [5, 6, 7, 8, 9, 10, 11, 12] in a series of papers. In particular, self-similar or quasi self-similar solutions describing the chemotactic collapse have been obtained and the formation of a Dirac peak has been found in the post-collapse regime in $d > 2$ and in the collapse regime in $d = 2$. In parallel, a vast number of rigorous results concerning the existence and unicity of solutions of the Keller-Segel model and the conditions of blow-up have been obtained by ap-

plied mathematicians (we refer to [13] for a connection to the mathematical literature).

In this paper, we consider novel aspects of the Keller-Segel model. We first introduce a regularized model that prevents finite time-blow up and the formation of (unphysical) singularities like infinite density profiles and Dirac peaks. In this model, the local density of cells is bounded by a maximum value $\rho(\mathbf{r}) \leq \sigma_0$ which takes into account finite size effects and filling factors. Therefore, the Dirac peaks (singularities) are replaced by smooth density profiles (clumps). With this regularization, there exists steady solutions (similar to the Fermi-Dirac distribution) for any value of the control parameter while the usual Keller-Segel model blows up above a critical mass $M > M_c$ (in dimension $d \geq 2$). In addition, we consider the limit of high degradation of the chemical. In this limit, we show that, for sufficiently small (effective) temperatures $T < T_c$, the system undergoes a second order phase transition from a homogeneous phase to an inhomogeneous phase. The bacteria organize in two domains with uniform density ρ_{\pm} separated by a thin interface. The resulting structure is similar to a "domain wall" in phase ordering kinetics [14]. We study in detail the structure of the interface (profile, width, surface tension,...) and determine the conditions for the bifurcation between a circular domain (spot) and a stripe in a square domain. This study can be performed analytically in the limit of high degradation (furthermore, our study is exact in $d = 1$). The case of a finite degradation rate will be treated numerically in another paper.

In previous papers [15, 4, 16], we have found a number of analogies between the chemotactic problem and other

systems of physical interest (self-gravitating systems, 2D vortices, Bose-Einstein condensation, Burgers equation). As mentioned previously, the Keller-Segel model is isomorphic to the Smoluchowski-Poisson system describing self-gravitating Brownian particles [5]. In this analogy, the concentration of the chemical produced by the bacteria plays a role similar to the gravitational potential in astrophysical systems (they are both solution of a Poisson equation) so that a number of analogies between biology and gravity can be developed [4]. In addition, the collapse of bacterial populations for $M > M_c$ or the collapse of self-gravitating Brownian particles for $T < T_c$ is by many respects similar to the Bose-Einstein condensation in phase space [16]. Finally, there exists some analogies between the chemotactic aggregation of bacteria and the formation of large-scale vortices in 2D turbulence [15,4]. In that case, the concentration of bacteria plays the role of the vorticity and the concentration of the chemical produced by the bacteria plays the role of the streamfunction. In two-dimensional hydrodynamics, the vorticity field which is solution of the 2D Euler equation can achieve a statistical equilibrium state (on the coarse-grained scale) as a result of turbulent mixing (violent relaxation) [17]. In the two-levels approximation, the equilibrium vorticity profile is given by a Fermi-Dirac-like distribution [18,19,20,21]. Interestingly, this is similar to the steady state of the regularized Keller-Segel model introduced in this paper. Furthermore, in the quasi-geostrophic (Q.G.) approximation relevant to geophysical flows [22], the finite value of the Rossby deformation radius introduces a shielding of the interaction between vortices which is formally similar to the degradation of the chemical in the chemotactic problem. In particular, the degradation rate k plays the same role as the inverse of the deformation radius R^{-1} . In the context of jovian vortices, Sommeria *et al.* [23] and Bouchet & Sommeria [24] have considered the limit of a small deformation radius $R \rightarrow 0$ to account for the annular jet structure of Jupiter's great red spot. As we shall see, this is similar to considering a limit of high degradation in the chemotactic problem. Therefore, many interesting results can be obtained by developing the analogies between these different topics.

The paper is organized as follows. In Sec. 2, we introduce a regularized Keller-Segel model of chemotactic aggregation. We first provide a phenomenological derivation of this model followed by a more kinetic approach. In Sec. 3, we study the equilibrium states of this model in a limit of high degradation. For $T < T_c$, we show that the solutions are formed by two phases in contact separated by an interface (the stability of the uniform phase is considered in Appendix A). In Secs. 3.1-3.3, we develop a "domain wall" theory to study the properties of the interface and determine its main characteristics (profile, width, surface tension,...). Asymptotic behaviors of these expressions are obtained for $T \rightarrow T_c$ and $T \rightarrow 0$ in Secs. 3.4 and 3.5. Analytical approximations of the jet profile are given in Secs. 3.6 and 3.7 in the form of self-similar solutions. Other approximations are given in Sec. 3.8 using match asymptotics. In Sec. 3.9, we show that the curvature ra-

dius is constant so that, in two dimensions, the interface is either a line (stripe) or a circle (spot). These results can be obtained equivalently by minimizing the free energy functional associated with the regularized Keller-Segel model (see Sec. 3.10). In Sec. 3.11, we determine the phase diagram of the system and the range of control parameters (B, T) where the equilibrium state is a stripe or a spot (the parameter B is related to the total mass of the configuration). Finally, in Sec. 4, we develop the close analogy between our biological system and the jet structure of Jupiter's great red spot and other jovian vortices.

2 The regularized Keller-Segel model

2.1 The dynamical equations

The general Keller-Segel model [3] describing the chemotaxis of bacterial populations consists in two coupled differential equations

$$\frac{\partial \rho}{\partial t} = \nabla \cdot (D_2 \nabla \rho) - \nabla \cdot (D_1 \nabla c), \quad (1)$$

$$\epsilon \frac{\partial c}{\partial t} = -k(c)c + f(c)\rho + D_c \Delta c, \quad (2)$$

that govern the evolution of the density of bacteria $\rho(\mathbf{r}, t)$ and the evolution of the secreted chemical $c(\mathbf{r}, t)$. The bacteria diffuse with a diffusion coefficient D_2 and they also move in a direction of a positive gradient of the chemical (chemotactic drift). The coefficient D_1 is a measure of the strength of the influence of the chemical gradient on the flow of bacteria. On the other hand, the chemical is produced by the bacteria with a rate $f(c)$ and is degraded with a rate $k(c)$. It also diffuses with a diffusion coefficient D_c . In the general Keller-Segel model, $D_1 = D_1(\rho, c)$ and $D_2 = D_2(\rho, c)$ can both depend on the concentration of the bacteria and of the chemical. This takes into account microscopic constraints, like close-packing effects, that can hinder the movement of bacteria.

A very much studied version of the Keller-Segel model is provided by the system of equations

$$\frac{\partial \rho}{\partial t} = \nabla \cdot (D \nabla \rho - \chi \rho \nabla c), \quad (3)$$

$$\epsilon \frac{\partial c}{\partial t} = D' \Delta c + a\rho - bc, \quad (4)$$

where the parameters are positive constants. Equation (3) can be viewed as a mean-field Fokker-Planck equation associated with a Langevin dynamics of the form

$$\frac{d\mathbf{r}}{dt} = \chi \nabla c + \sqrt{2D} \mathbf{R}(t), \quad (5)$$

where $\mathbf{R}(t)$ is a white noise and χ plays the role of a mobility. The stationary solution of Eq. (3) is given by

$$\rho = A e^{\frac{\chi}{D} c}. \quad (6)$$

This is similar to the Boltzmann distribution for a system in a potential $-c$. This suggests to introducing an effective temperature through the relation $T_{eff} = D/\chi$ which is similar to the Einstein relation. For $\epsilon = 0$, the system (3)-(4) monotonically decreases ($\dot{F} \leq 0$) the Lyapunov functional

$$F = -\frac{1}{2} \int \rho c \, d\mathbf{r} + \frac{D}{\chi} \int \rho \ln \rho \, d\mathbf{r}, \quad (7)$$

which is similar to a free energy $F = E - T_{eff}S$ where $E = -\frac{1}{2} \int \rho c \, d\mathbf{r}$ is the energy of interaction and $S = -\int \rho \ln \rho \, d\mathbf{r}$ is the Boltzmann entropic functional¹. For $\epsilon \neq 0$, the Lyapunov functional is

$$F = \frac{1}{2a} \int [D'(\nabla c)^2 + bc^2] \, d\mathbf{r} - \int \rho c \, d\mathbf{r} + \frac{D}{\chi} \int \rho \ln \rho \, d\mathbf{r}. \quad (8)$$

We shall consider here a more general situation where the mobility and the diffusion coefficient in the Keller-Segel model can depend on the density of bacteria. In that case, Eq. (3) is replaced by

$$\frac{\partial \rho}{\partial t} = \nabla \cdot [\nabla(D(\rho)\rho) - \chi(\rho)\rho \nabla c]. \quad (9)$$

This can be viewed as a nonlinear mean-field Fokker-Planck equation [15]. It is associated with a Langevin equation of the form

$$\frac{d\mathbf{r}}{dt} = \chi(\rho)\nabla c + \sqrt{2D(\rho)}\mathbf{R}(t). \quad (10)$$

We define the functions h and g by

$$Dh(\rho) = \frac{d}{d\rho}(\rho D(\rho)), \quad (11)$$

$$\chi g(\rho) = \rho \chi(\rho), \quad (12)$$

where D and χ are positive coefficients. With these notations, Eq. (9) can be rewritten

$$\frac{\partial \rho}{\partial t} = \nabla \cdot [Dh(\rho)\nabla \rho - \chi g(\rho)\nabla c]. \quad (13)$$

Setting $\beta = 1/T_{eff} = \chi/D$, we obtain

$$\frac{\partial \rho}{\partial t} = \nabla \cdot [D(h(\rho)\nabla \rho - \beta g(\rho)\nabla c)]. \quad (14)$$

This type of nonlinear mean-field Fokker-Planck equations has been discussed in [15]. They are associated with generalized entropic functionals of the form

$$S = - \int C(\rho) \, d\mathbf{r}, \quad (15)$$

¹ Note that these analogies with thermodynamics take even more sense if we remark that the Keller-Segel model is isomorphic to the Smoluchowski-Poisson system for self-gravitating Brownian particles [4].

where $C(\rho)$ is a convex function defined by

$$C''(\rho) = \frac{h(\rho)}{g(\rho)}. \quad (16)$$

The Keller-Segel model (3)-(4) is known to exhibit blow-up solutions when the chemotactic attraction prevails over diffusion [13,10]. This reproduces the chemotactic aggregation of bacterial populations. In theory, the density can take arbitrarily large values and ultimately forms a Dirac peak. In reality, this singular evolution is unphysical as we expect finite size effects and close-packing effects to become important when the system aggregates and becomes dense enough. We shall regularize the problem by introducing a sort of filling factor in the drift-diffusion equation (14). Thus, we take $h(\rho) = 1$ and $g(\rho) = \rho(1 - \rho/\sigma_0)$ so that Eq. (3) is replaced by

$$\frac{\partial \rho}{\partial t} = \nabla \cdot [D(\nabla \rho - \beta \rho(1 - \rho/\sigma_0)\nabla c)]. \quad (17)$$

With this modification, the mobility is reduced when the density becomes high enough (i.e. when ρ approaches the value σ_0) and this prevents singularities to form. Indeed, it can be shown that the density remains always bounded: $\rho(\mathbf{r}, t) \leq \sigma_0$. This bound is similar to the Pauli exclusion principle in quantum mechanics, but it occurs here in physical space. The regularized drift-diffusion equation (17) was introduced phenomenologically in [15,4] to avoid infinite values of the density.

In the following, we shall take $\epsilon = 0$ for simplicity (although many results which are valid at equilibrium are independent on this assumption). This is valid in a limit of high diffusivity of the chemical [25]. If we introduce the notations $k^2 = b/D'$ and $\lambda = a/D'$, we obtain the regularized Keller-Segel model

$$\frac{\partial \rho}{\partial t} = \nabla \cdot [D(\nabla \rho - \beta \rho(1 - \rho/\sigma_0)\nabla c)], \quad (18)$$

$$\Delta c - k^2 c = -\lambda \rho. \quad (19)$$

The stationary solution of Eq. (18) is given by

$$\rho = \frac{\sigma_0}{1 + e^{-\beta c + \alpha}}, \quad (20)$$

which is similar to the Fermi-Dirac distribution in physical space. From this expression, we clearly have $\rho(\mathbf{r}) \leq \sigma_0$. Furthermore, the Lyapunov functional can be written in the form of a free energy $F = E - T_{eff}S$ where

$$E = -\frac{1}{2} \int \rho c \, d\mathbf{r} = -\frac{1}{2\lambda} \int [(\nabla c)^2 + k^2 c^2] \, d\mathbf{r}, \quad (21)$$

is the energy of interaction and

$$S = -\sigma_0 \int \left\{ \frac{\rho}{\sigma_0} \ln \frac{\rho}{\sigma_0} + \left(1 - \frac{\rho}{\sigma_0}\right) \ln \left(1 - \frac{\rho}{\sigma_0}\right) \right\} \, d\mathbf{r}, \quad (22)$$

is the Fermi-Dirac entropic functional in physical space. The distribution (20) extremizes the free energy at fixed mass. Indeed, writing the first order variations in the form $\delta F + \alpha T_{eff} \delta M = 0$ where α is a Lagrange multiplier, we recover Eq. (20). Furthermore, it can be shown that a stationary solution of Eqs. (18)-(19) is linearly stable if, and only if, it is a *minimum* of F at fixed mass [15].

2.2 Phenomenological derivation of the model

In this section, we develop a connection between the chemotactic problem and thermodynamics. To that purpose, we introduce the entropic functional (22) from a combinatorial analysis which respects an exclusion principle in physical space. Then, we obtain the dynamical equation (18) from arguments similar to the linear thermodynamics of Onsager.

We divide the domain into a very large number of microcells with size h . We assume that the size h is of the order of the size of a particle so that a microcell is occupied either by 0 or 1 particle. This is how the exclusion principle is introduced in the problem. We shall now group these microcells into macrocells each of which contains many microcells but remains nevertheless small compared to the spatial extension of the whole system. We call ν the number of microcells in a macrocell. Consider the configuration $\{n_i\}$ where there are n_1 particles in the 1st macrocell, n_2 in the 2nd macrocell etc..., each occupying one of the ν microcells with no cohabitation. The number of ways of assigning a microcell to the first element of a macrocell is ν , to the second $\nu - 1$ etc. Assuming that the particles are indistinguishable, the number of ways of assigning microcells to all n_i particles in a macrocell is thus

$$\frac{1}{n_i!} \times \frac{\nu!}{(\nu - n_i)!}. \quad (23)$$

To obtain the number of microstates corresponding to the macrostate $\{n_i\}$ defined by the number of particles n_i in each macrocell (irrespective of their precise position in the cell), we need to take the product of terms such as (23) over all macrocells. Thus, the number of microstates corresponding to the macrostate $\{n_i\}$, which is proportional to the *a priori* probability of the state $\{n_i\}$, is

$$W(\{n_i\}) = \prod_i \frac{\nu!}{n_i!(\nu - n_i)!}. \quad (24)$$

This is the Fermi-Dirac statistics which is applied here in physical space. As is customary, we define the entropy of the state $\{n_i\}$ by

$$S(\{n_i\}) = \ln W(\{n_i\}). \quad (25)$$

It is convenient here to return to a representation in terms of the density in the i -th macrocell

$$\rho_i = \rho(\mathbf{r}_i) = \frac{n_i}{\nu} \frac{m}{h^d} = \frac{n_i \sigma_0}{\nu}, \quad (26)$$

where we have defined $\sigma_0 = m/h^d$, which represents the maximum value of ρ due to the exclusion constraint. Now, using the Stirling formula, we have

$$\begin{aligned} \ln W(\{n_i\}) \simeq & \sum_i \nu (\ln \nu - 1) - \nu \left\{ \frac{\rho_i}{\sigma_0} \left[\ln \left(\frac{\nu \rho_i}{\sigma_0} \right) - 1 \right] \right. \\ & \left. + \left(1 - \frac{\rho_i}{\sigma_0} \right) \left[\ln \left\{ \nu \left(1 - \frac{\rho_i}{\sigma_0} \right) \right\} - 1 \right] \right\}. \end{aligned} \quad (27)$$

Passing to the continuum limit $\nu \rightarrow 0$, we obtain the expression (21) of the Fermi-Dirac entropy in physical space. In the dilute limit $\rho \ll \sigma_0$, it reduces to the Boltzmann entropy (7).

The entropy is the correct thermodynamical potential for an isolated system for which the energy is conserved (microcanonical ensemble). This is not the case for our system which is dissipative. The proper description is the canonical ensemble and the correct thermodynamical potential is the free energy $F = E - T_{eff} S$ constructed with the Fermi-Dirac entropy (22) and the energy (21). The equilibrium state in the canonical ensemble is obtained by minimizing the free energy at fixed mass. Writing the first variations as $\delta F - \lambda \delta M = 0$, we obtain

$$\frac{\delta F}{\delta \rho} - \lambda = 0, \quad (28)$$

which leads to the Fermi-Dirac distribution (20) with $\alpha = -\lambda\beta$. Now that the proper thermodynamical potential has been derived by a combinatorial analysis, we can introduce phenomenologically a dynamical model by writing the evolution of the density as a continuity equation $\partial_t \rho = \nabla \cdot \mathbf{J}$ where the current is the gradient of the functional derivative of the free energy, i.e.

$$\frac{\partial \rho}{\partial t} = \nabla \cdot \left(\mu \nabla \frac{\delta F}{\delta \rho} \right). \quad (29)$$

This formulation ensures that the free energy decreases monotonically provided that $\mu \geq 0$. Indeed,

$$\begin{aligned} \dot{F} &= \int \frac{\delta F}{\delta \rho} \frac{\partial \rho}{\partial t} d\mathbf{r} = \int \frac{\delta F}{\delta \rho} \nabla \cdot \mathbf{J} d\mathbf{r} \\ &= - \int \mathbf{J} \cdot \nabla \frac{\delta F}{\delta \rho} d\mathbf{r} = - \int \mu \left(\nabla \frac{\delta F}{\delta \rho} \right)^2 d\mathbf{r} \leq 0. \end{aligned} \quad (30)$$

Furthermore, a steady state satisfies $\dot{F} = 0$, i.e $\nabla(\delta F/\delta \rho) = 0$ leading to Eq. (28). Now, using Eqs. (21) and (22), we have

$$\nabla \frac{\delta F}{\delta \rho} = -\nabla c + \frac{D}{\chi} \frac{\nabla \rho}{\rho(1 - \rho/\sigma_0)}. \quad (31)$$

To avoid the singularity when $\rho = 0$ or $\rho = \sigma_0$, we require that μ is proportional to $\rho(1 - \rho/\sigma_0)$. Writing Eq. (29) in the form

$$\frac{\partial \rho}{\partial t} = \nabla \cdot \left[\chi \rho (1 - \rho/\sigma_0) \nabla \frac{\delta F}{\delta \rho} \right], \quad (32)$$

and using Eq. (31), we obtain Eq. (17). This approach to construct relaxation equations is equivalent to Onsager's linear thermodynamics. Indeed, noting that the potential

$$\lambda(\mathbf{r}, t) \equiv \frac{\delta F}{\delta \rho} = -c + T_{eff} \ln \left(\frac{\rho/\sigma_0}{1 - \rho/\sigma_0} \right), \quad (33)$$

is uniform at equilibrium according to Eq. (20) or (28), the linear thermodynamics of Onsager suggests to writing the current as

$$\mathbf{J} = \mu \nabla \lambda(\mathbf{r}, t), \quad (34)$$

which is equivalent to Eq. (29). The same results can be obtained by a variational formulation which is related to the Maximum Entropy Production Principle (MEPP) [15]. The rate of dissipation of free energy is given by

$$\dot{F} = \int \frac{\delta F}{\delta \rho} \frac{\partial \rho}{\partial t} d\mathbf{r} = \int \frac{\delta F}{\delta \rho} \nabla \cdot \mathbf{J} d\mathbf{r} = - \int \mathbf{J} \cdot \nabla \frac{\delta F}{\delta \rho} d\mathbf{r}. \quad (35)$$

We shall determine the optimal current \mathbf{J}_* which maximizes the rate of dissipation of free energy \dot{F} under the constraint $J^2 \leq C(\mathbf{r}, t)$ putting a (physical) bound on $|\mathbf{J}|$. The corresponding variational problem can be written

$$\delta \dot{F} + \delta \int \frac{\mathbf{J}^2}{2\mu} d\mathbf{r} = 0, \quad (36)$$

where μ is a Lagrange multiplier. Performing the variations on \mathbf{J} , we obtain $\mathbf{J}_* = \mu \nabla (\delta F / \delta \rho)$ which returns Eq. (29).

2.3 Kinetic derivation of the model

As discussed previously, Eq. (14) can be viewed as a non-linear Fokker-Planck equation where the diffusion coefficient and the mobility explicitly depend on the local concentration of particles. Such generalized Fokker-Planck equations can be derived from a kinetic theory, starting from the master equation, and assuming that the probabilities of transition explicitly depend on the occupation number (concentration) of the initial and arrival states. Below, we briefly summarize and adapt to the present situation the approach carried out by Kaniadakis [26] in a more general context.

We introduce a stochastic dynamics by defining the probability of transition of a bacteria from position \mathbf{r} to position \mathbf{r}' . Following Kaniadakis [26], we assume the following form

$$\pi(\mathbf{r} \rightarrow \mathbf{r}') = w(\mathbf{r}, \mathbf{r} - \mathbf{r}') a[\rho(\mathbf{r}, t)] b[\rho(\mathbf{r}', t)]. \quad (37)$$

Usual stochastic processes correspond to $a(\rho) = \rho$ and $b(\rho) = 1$: the probability of transition is proportional to the density of the initial state and independent on the density of the final state. They lead to the Fokker-Planck equation (3) as will be shown below. Here, we assume a more general dependence on the occupancy in the initial

and arrival states. This can account for microscopic constraints like close-packing effects that can inhibit the transition. Quite generally, the evolution of the density satisfies the master equation

$$\frac{\partial \rho}{\partial t} = \int [\pi(\mathbf{r}' \rightarrow \mathbf{r}) - \pi(\mathbf{r} \rightarrow \mathbf{r}')] d\mathbf{r}'. \quad (38)$$

Assuming that the evolution is sufficiently slow, and local, such that the dynamics only permits values of \mathbf{r}' close to \mathbf{r} , one can develop the term in brackets in Eq. (38) in powers of $\mathbf{r} - \mathbf{r}'$. Proceeding along the lines of [26], we obtain a Fokker-Planck-like equation

$$\frac{\partial \rho}{\partial t} = \frac{\partial}{\partial x_i} \left[\left(\zeta_i + \frac{\partial \zeta_{ij}}{\partial x_j} \right) \gamma(\rho) + \gamma(\rho) \frac{\partial \ln \kappa(\rho)}{\partial \rho} \zeta_{ij} \frac{\partial \rho}{\partial x_j} \right], \quad (39)$$

with

$$\gamma(\rho) = a(\rho)b(\rho), \quad \kappa(\rho) = \frac{a(\rho)}{b(\rho)}, \quad (40)$$

and

$$\zeta_i(\mathbf{r}) = - \int y_i w(\mathbf{r}, \mathbf{y}) d\mathbf{y}, \quad (41)$$

$$\zeta_{ij}(\mathbf{r}) = \frac{1}{2} \int y_i y_j w(\mathbf{r}, \mathbf{y}) d\mathbf{y}. \quad (42)$$

The moments ζ_i and ζ_{ij} are fixed by the Langevin equations (5). Assuming isotropy

$$\zeta_i = J_i, \quad \zeta_{ij} = D \delta_{ij}, \quad (43)$$

the kinetic equation becomes

$$\frac{\partial \rho}{\partial t} = \nabla \cdot \left[(\mathbf{J} + \nabla D) \gamma(\rho) + \gamma(\rho) \frac{\partial \ln \kappa(\rho)}{\partial \rho} D \nabla \rho \right]. \quad (44)$$

Now, according to the Langevin equations (5), D is independent on \mathbf{r} and $\mathbf{J} = -\chi \nabla c$. Thus, we get

$$\frac{\partial \rho}{\partial t} = \nabla \cdot \left[D \gamma(\rho) \frac{\partial \ln \kappa(\rho)}{\partial \rho} \nabla \rho - \chi \gamma(\rho) \nabla c \right]. \quad (45)$$

If we define

$$h(\rho) = \gamma(\rho) \frac{\partial \ln \kappa(\rho)}{\partial \rho}, \quad g(\rho) = \gamma(\rho), \quad (46)$$

the foregoing equation can be written

$$\frac{\partial \rho}{\partial t} = \nabla \cdot [D h(\rho) \nabla \rho - \chi g(\rho) \nabla c], \quad (47)$$

and it coincides with the phenomenological equation (13). It seems natural to assume that the transition probability is proportional to the density of the initial state so that $a(\rho) = \rho$. In that case, we obtain an equation of the form

$$\frac{\partial \rho}{\partial t} = \nabla \cdot (D [b(\rho) - \rho b'(\rho)] \nabla \rho - \chi \rho b(\rho) \nabla c). \quad (48)$$

Note that the coefficients of diffusion and mobility are not independent since they are both expressed in terms

of $b(\rho)$. Choosing $b(\rho) = 1$, i.e. a probability of transition which does not depend on the population of the arrival state, leads to the standard Fokker-Planck equation (3). If, now, we assume that the transition probability is blocked (inhibited) if the concentration of the arrival state is equal to σ_0 , then it seems natural to take $b(\rho) = 1 - \rho/\sigma_0$. In that case, we obtain

$$\frac{\partial \rho}{\partial t} = \nabla \cdot (D \nabla \rho - \chi \rho (1 - \rho/\sigma_0) \nabla c), \quad (49)$$

which coincides with the phenomenological equation (17).

We can consider a related kinetic model with similar thermodynamical properties and the same equilibrium states. For this model, the dynamical equation reads

$$\frac{\partial \rho}{\partial t} = \nabla \cdot \left[\chi \left(\frac{T_{eff}}{1 - \rho/\sigma_0} \nabla \rho - \rho \nabla c \right) \right]. \quad (50)$$

This can be put in the form of a generalized Smoluchowski equation [15]:

$$\frac{\partial \rho}{\partial t} = \nabla \cdot \left[\frac{1}{\xi} (\nabla p - \rho \nabla c) \right], \quad (51)$$

associated with a barotropic equation of state $p(\rho) = -\sigma_0 T_{eff} \ln(1 - \rho/\sigma_0)$, where p is an effective ‘‘pressure’’. For $\rho \ll \sigma_0$, we recover the ‘‘isothermal’’ equation of state $p = \rho T_{eff}$ leading to the ordinary Keller-Segel model (3).

Equations (49) and (50) have very similar properties and they can be viewed as natural extensions of the Keller-Segel model. In Eq. (49) the regularization is put in the drift term while in Eq. (50) it is put in the diffusion term. These two possibilities are considered in [15]. Note finally that Eq. (50) can be obtained from the master equation (38) when the transition probabilities are of the form (37) with $a(\rho) = \rho/\sqrt{1 - \rho/\sigma_0}$ and $b(\rho) = \sqrt{1 - \rho/\sigma_0}$.

3 Domain wall theory

3.1 The stationary state

The stationary solution of the regularized Keller-Segel model (18) is the Fermi-Dirac-like distribution

$$\rho = \frac{\sigma_0}{1 + e^{-\beta c + \alpha}}. \quad (52)$$

This relates, at equilibrium, the bacterial density ρ to the concentration of the chemical c . The chemical is itself produced by the bacteria according to Eq. (19). Thus, combining Eqs. (52) and (19), we obtain a differential equation for the concentration c . Using the identity

$$\frac{1}{1 + e^x} = \frac{1}{2} \left[1 - \tanh \left(\frac{x}{2} \right) \right], \quad (53)$$

this mean-field equation can be written

$$\Delta c - k^2 c = -\frac{\lambda \sigma_0}{2} \left[1 - \tanh \left(\frac{\alpha - \beta c}{2} \right) \right]. \quad (54)$$

Introducing the new variables

$$\psi = \frac{c}{(\lambda \sigma_0 / 2)}, \quad \mu = \frac{\alpha}{2}, \quad C = \frac{\beta \lambda \sigma_0}{4k^2}, \quad (55)$$

we get

$$\Delta \psi - k^2 \psi = -1 + \tanh \left[C \left(\frac{\mu}{C} - k^2 \psi \right) \right]. \quad (56)$$

We shall solve this equation perturbatively in a limit of high degradation so that $k \gg 1$ (note that the following treatment is exact in 1D without approximation). In that limit, we can neglect the gradient of concentration except in a thin layer of length $\sim k^{-1}$ (domain wall) where the concentration changes rapidly. Outside the wall, we obtain the algebraic equation

$$-k^2 \psi = -1 + \tanh \left[C \left(\frac{\mu}{C} - k^2 \psi \right) \right]. \quad (57)$$

In some range of parameters (see below), this equation determines two solutions ψ_{\pm} which correspond to two phases with uniform concentration. These two phases are connected by a ‘‘wall’’. For $k \gg 1$, the interface is very thin so that we can neglect the curvature of the wall in a first approximation. The wall profile is then determined by the one-dimensional differential equation

$$\frac{d^2 \psi}{d\xi^2} - k^2 \psi = -1 + \tanh \left[C \left(\frac{\mu}{C} - k^2 \psi \right) \right], \quad (58)$$

where ξ is a coordinate normal to the interface.

3.2 The wall equation

If we set

$$\phi = k^2 \psi - \mu/C, \quad \tau = k\xi, \quad \chi = \frac{\mu}{C} - 1, \quad (59)$$

we obtain the wall equation

$$\frac{d^2 \phi}{d\tau^2} = -\tanh(C\phi) + \phi + \chi. \quad (60)$$

Eq. (60) is similar to the equation of motion for a particle in a potential

$$U(\phi) = T \ln [\cosh(\phi/T)] - \frac{\phi^2}{2} + \chi\phi + U_0, \quad (61)$$

where τ plays the role of time and ϕ plays the role of position. Indeed, it can be rewritten

$$\frac{d^2 \phi}{d\tau^2} = -U'(\phi). \quad (62)$$

We have introduced the notation $C = 1/T$ where, as we shall see, T plays the role of a temperature (it is furthermore proportional to the effective temperature T_{eff}). On the other hand, U_0 is a constant of integration that will be specified later.

Far from the wall, the density is uniform with values ϕ_{\pm} satisfying

$$U'(\phi_{\pm}) = 0. \quad (63)$$

On the other hand, a first integral of Eq. (62) is

$$E = \frac{1}{2} \left(\frac{d\phi}{d\tau} \right)^2 + U(\phi). \quad (64)$$

The condition of solvability is therefore

$$U(\phi_-) = U(\phi_+). \quad (65)$$

The only possibility to satisfy the two conditions (63)-(65) simultaneously is that $\chi = 0$, i.e. $\mu = \frac{1}{T}$ (in that case, $U(\phi)$ is symmetric and the above conditions are satisfied trivially). Then, the wall profile is completely determined by the equations

$$\frac{d^2\phi}{d\tau^2} = -\tanh(\phi/T) + \phi, \quad (66)$$

$$U(\phi) = T \ln [\cosh(\phi/T)] - \frac{\phi^2}{2} + U_0, \quad (67)$$

$$\phi_{\pm} = \pm u, \quad u = \tanh(u/T). \quad (68)$$

We note that the algebraic equation has solutions $u \neq 0$ only if (see Fig. 1)

$$T < T_c = 1. \quad (69)$$

This is similar to a second order phase transition (see Fig. 2). In that case, the algebraic equation has three solutions 0 and $\pm u$ with $u \leq 1$ (but the solution $\phi = u = 0$ is unstable). The concentrations of bacteria and chemical in the uniform domains are related to the order parameter u by

$$c_{\pm} = \frac{\lambda\sigma_0}{2k^2} (1 \pm u), \quad \rho_{\pm} = \frac{\sigma_0}{2} (1 \pm u). \quad (70)$$

More generally, using Eqs. (52)-(53) the concentration profiles in the whole space can be expressed in terms of the field ϕ by

$$c = \frac{\lambda\sigma_0}{2k^2} (1 + \phi), \quad \rho = \frac{\sigma_0}{2} [1 - \tanh(\phi/T)]. \quad (71)$$

3.3 The wall profile

We determine U_0 such that $U(u) = 0$. The potential is then explicitly given by (see Fig. 3):

$$U(\phi) = T \ln \left[\cosh \left(\frac{\phi}{T} \right) \right] - \frac{\phi^2}{2} - T \ln \left[\cosh \left(\frac{u}{T} \right) \right] + \frac{u^2}{2}. \quad (72)$$

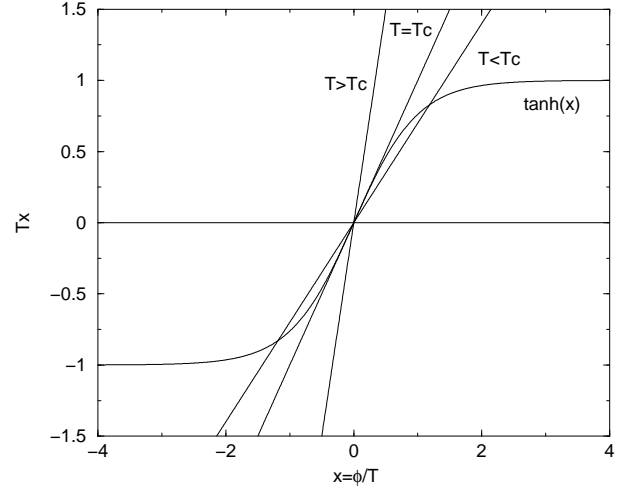


Fig. 1. Graphical construction determining the solutions $\pm u$ of the algebraic equation (68)-b as a function of the temperature T .

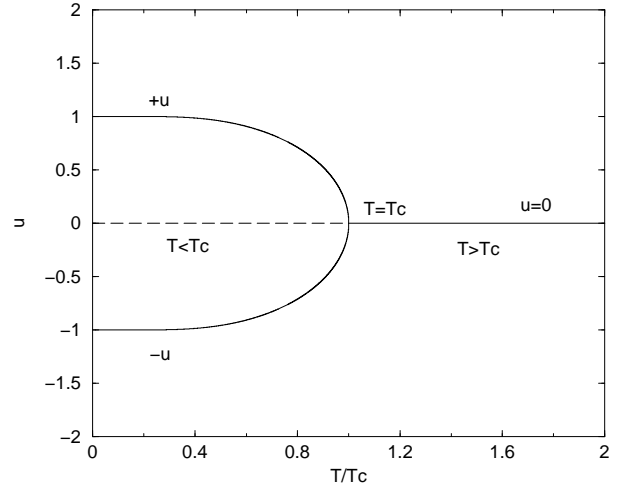


Fig. 2. Evolution of the order parameter u as a function of the temperature T . For $T > T_c$ the system is homogeneous with $\phi = u = 0$. For $T < T_c$, the uniform solution becomes unstable (see Appendix A) and two phases $\phi_{\pm} = \pm u$ separated by a “domain wall” appear.

With this convention, the constant appearing in Eq. (64) is $E = 0$. Then, we obtain the equation

$$\frac{1}{2} \left(\frac{d\phi}{d\tau} \right)^2 = -U(\phi), \quad (73)$$

which determines the wall profile by a simple integration (see Fig. 4)

$$\int_0^{\phi} \frac{dx}{\sqrt{-2U(x)}} = \tau. \quad (74)$$

For $\tau \rightarrow +\infty$, $\phi \rightarrow u$. To get the asymptotic behaviour, we set $\phi = u - \theta$ with $\theta \ll 1$ and we linearize the wall

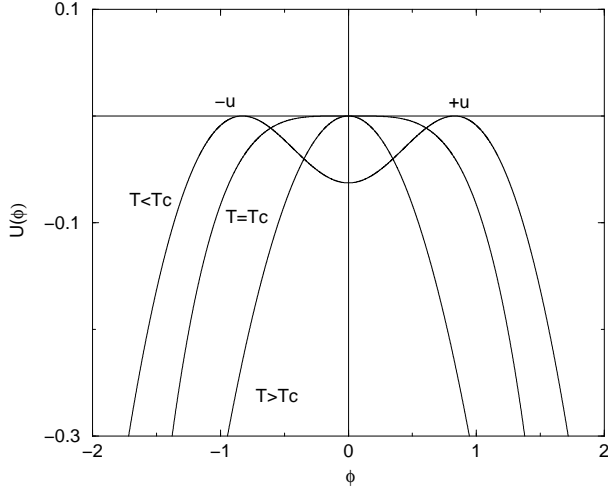


Fig. 3. The potential $U(\phi)$ of the equivalent mechanical problem for different values of the temperature.

equation (73). This yields

$$\frac{d\theta}{d\tau} = -\sqrt{-U''(u)}\theta, \quad (75)$$

with $U''(u) = \frac{1}{T}(1-u^2) - 1 < 0$ for $T < T_c$. The wall connects the uniform phase exponentially rapidly. Thus, we can write

$$\phi = u - A(u)e^{-2\tau/L(u)}, \quad (\tau \rightarrow +\infty) \quad (76)$$

where the typical width of the wall (expressed in units of k^{-1}) is

$$L(u) = \frac{2}{\sqrt{-U''(u)}} = \frac{2}{\sqrt{1 - \frac{1}{T}(1-u^2)}}. \quad (77)$$

We introduce the concentration gradient (see Fig. 5)

$$v(\tau) = \frac{d\phi}{d\tau} = \sqrt{-2U(\phi)}. \quad (78)$$

Using Eq. (72), we find that the maximum value of the concentration gradient, corresponding to $\phi = 0$, is given by

$$v_{max}(u) = \sqrt{2T \ln \left[\cosh \left(\frac{u}{T} \right) \right] - u^2}. \quad (79)$$

Finally, the energy of the wall, or surface tension, is

$$\sigma(u) = \int_{-\infty}^{+\infty} \left(\frac{d\phi}{d\tau} \right)^2 d\tau = \int_{-u}^{+u} \sqrt{-2U(\phi)} d\phi. \quad (80)$$

The functions L , σ and v_{max} are plotted in Figs. 6, 7 and 8 as a function of the temperature T , together with their asymptotic expressions computed in the following sections. The concentration profiles of bacteria and of the secreted chemical, given by Eq. (71), are plotted in Fig. 9.

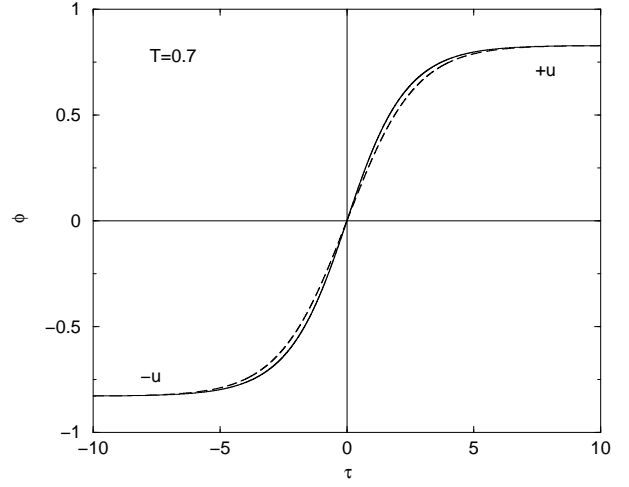


Fig. 4. Plot of the field ϕ across the wall for $T = 0.7$. The solid line corresponds to the exact solution of Eq. (73) obtained numerically and the dashed line corresponds to the approximate expression (100).

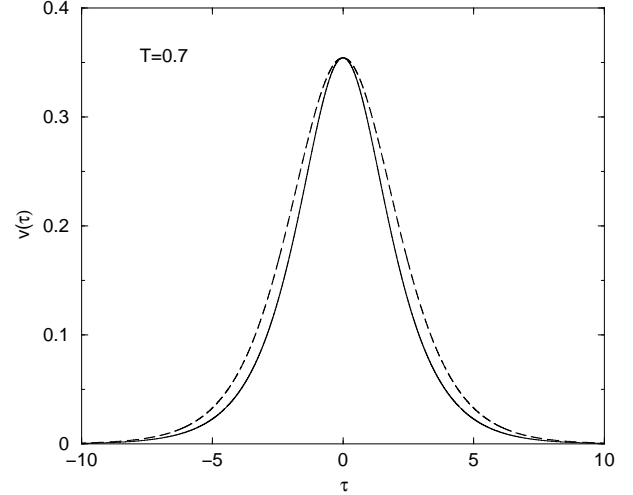


Fig. 5. Plot of the concentration gradient $v(\tau)$ across the wall for $T = 0.7$. The solid line corresponds to the exact solution of Eq. (73) obtained numerically and the dashed line corresponds to the approximate expression (103)-(105).

3.4 The limit $T \rightarrow T_c$

For $T \rightarrow T_c$, $u \rightarrow 0$ and $\phi \ll 1$. In that case, we can expand the potential to order ϕ^4 to obtain

$$U(\phi) = \frac{1}{2}(1-T)\phi^2 - \frac{1}{12}\phi^4 + U_0. \quad (81)$$

The wall equation becomes

$$\frac{d^2\phi}{d\tau^2} = -(1-T)\phi + \frac{1}{3}\phi^3. \quad (82)$$

The uniform solutions are $\phi = 0$ and $\phi^2 = 3(1-T)$ yielding

$$u = \sqrt{3(1-T)}. \quad (83)$$

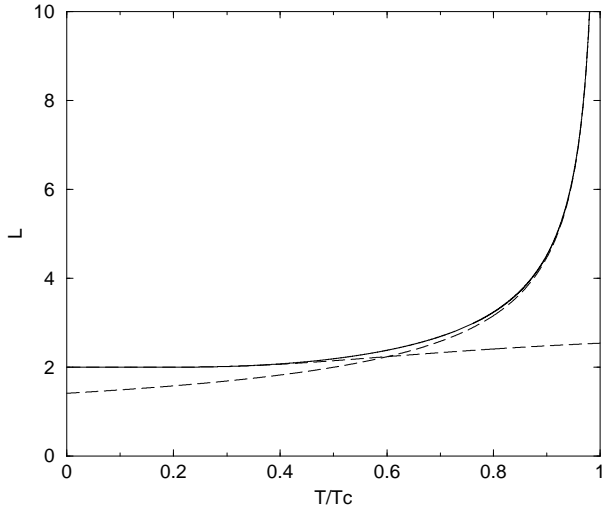


Fig. 6. Evolution of the typical width of the wall as a function of the temperature. The dashed lines correspond to the asymptotic expressions for $T \rightarrow 0$ and $T \rightarrow T_c$.

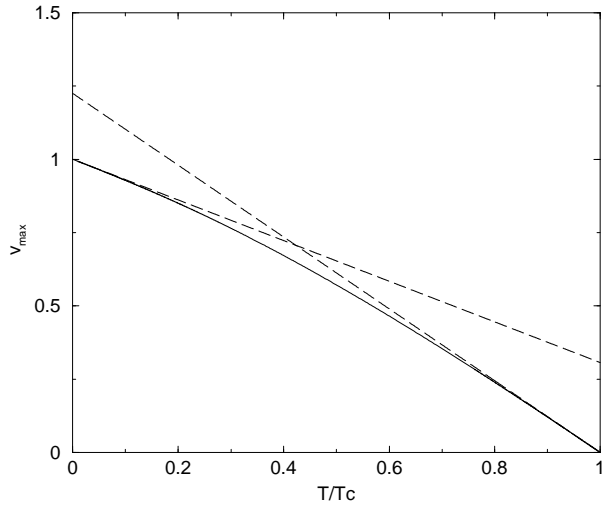


Fig. 7. Evolution of the maximum concentration gradient as a function of the temperature. The dashed lines correspond to the asymptotic expressions for $T \rightarrow 0$ and $T \rightarrow T_c$.

We can now re-express the potential in the form

$$U(\phi) = -\frac{1}{12}(\phi^2 - u^2)^2. \quad (84)$$

The wall profile is given by

$$\int \frac{d\phi}{u^2 - \phi^2} = \frac{\tau}{\sqrt{6}}, \quad (85)$$

yielding explicitly

$$\phi = u \tanh\left(\frac{u\tau}{\sqrt{6}}\right). \quad (86)$$

The typical width of the wall, as defined by Eq. (77), is

$$L = \frac{\sqrt{6}}{u} = \sqrt{2}(1-T)^{-1/2}. \quad (87)$$

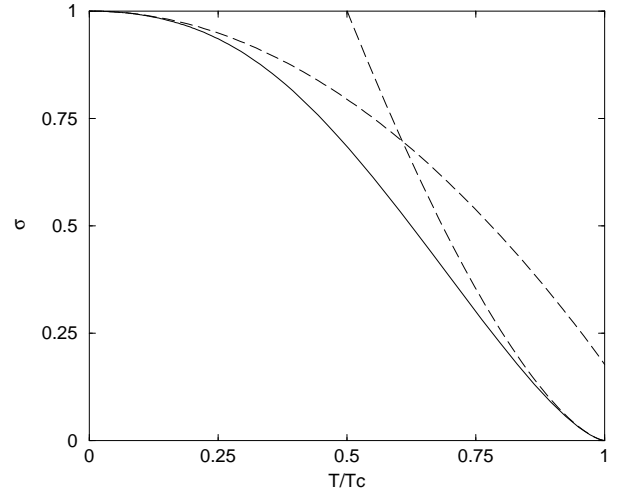


Fig. 8. Evolution of the energy of the wall (surface tension) as a function of the temperature. The dashed lines correspond to the asymptotic expressions for $T \rightarrow 0$ and $T \rightarrow T_c$.

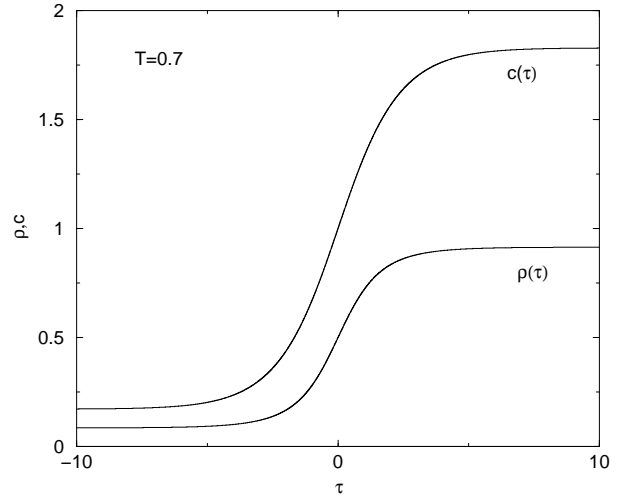


Fig. 9. Concentration profiles of bacteria ρ (in units of σ_0) and of the secreted chemical c (in units of $\lambda\sigma_0/2k^2$) for $T = 0.7$.

The width of the wall diverges at the critical point with the exponent $-1/2$. The wall profile can be rewritten

$$\phi = u(T) \tanh\left[\frac{\tau}{L(T)}\right], \quad (88)$$

and the concentration gradient is

$$v(\tau) = \frac{u(T)}{L(T)} \cosh^{-2}\left[\frac{\tau}{L(T)}\right]. \quad (89)$$

The maximum value of the concentration gradient is given by

$$v_{max} = \frac{u^2}{\sqrt{6}} = \left(\frac{3}{2}\right)^{1/2} (1-T), \quad (90)$$

and it tends to zero with the exponent +1 at the critical temperature. Finally, the surface tension is given by

$$\sigma = \left(\frac{2}{3}\right)^{3/2} u^3 = [2(1-T)]^{3/2}, \quad (91)$$

and it vanishes at the critical point with the exponent +3/2. These are the same scalings as in the Cahn-Hilliard theory [27].

3.5 The limit $T \rightarrow 0$

Setting $x = u/T$, Eq. (68)-b can be rewritten $Tx = \tanh(x)$. For $T \rightarrow 0$, $x \sim 1/T \rightarrow +\infty$ and $u \rightarrow 1$. More precisely, considering the behavior of $\tanh(x)$ for $x \rightarrow +\infty$, we get

$$u \simeq 1 - 2e^{-2/T}. \quad (92)$$

The potential can be rewritten (for $\phi \geq 0$)

$$U(\phi) = \phi + Te^{-2\phi/T} - \frac{\phi^2}{2} + U_0. \quad (93)$$

The typical width of the wall is

$$L = 2 \left(1 + \frac{2}{T}e^{-2/T}\right) = 2 - (1-u) \ln \left(\frac{1-u}{2}\right), \quad (94)$$

and the maximum value of the concentration gradient is

$$v_{max} = 1 - (\ln 2)T = 1 - \frac{2 \ln 2}{\ln \left(\frac{1-u}{2}\right)}. \quad (95)$$

Finally, the surface tension is given by (see Appendix B)

$$\sigma = 1 - \frac{\pi^2}{12}T^2 = 1 - \frac{\pi^2}{6 \ln \left(\frac{1-u}{2}\right)}. \quad (96)$$

For $T = 0$, we have $u = 1$ and

$$U(\phi) = \phi - \frac{\phi^2}{2} - \frac{1}{2} = -\frac{1}{2}(\phi - 1)^2. \quad (97)$$

The wall profile is solution of

$$\frac{d\phi}{d\tau} = 1 - \phi, \quad (98)$$

leading to

$$\phi = 1 - e^{-\tau} \quad (\tau \geq 0). \quad (99)$$

3.6 Simple approximation for $T > 1/2$

If we are relatively close to the critical temperature, we can propose a simple approximation of the wall profile in the form

$$\phi = u(T) \tanh \left[\frac{\tau}{L(T)} \right], \quad (100)$$

where u and L are given by the *exact* expressions

$$u = \tanh \left(\frac{u}{T} \right), \quad (101)$$

$$L = \frac{2}{\sqrt{1 - \frac{1}{T}(1-u^2)}}. \quad (102)$$

This Ansatz becomes exact when $T \rightarrow T_c$ and it provides a fair approximation for smaller temperatures (typically $T > 1/2$), see Fig. 4.

The concentration gradient obtained from Eq. (100) is given by

$$v(\tau) = \frac{v_{max}(T)}{\cosh^2(\tau/L(T))}, \quad (103)$$

with the maximum value

$$v_{max} = \frac{u}{L} = \frac{u}{2} \sqrt{1 - \frac{1}{T}(1-u^2)}. \quad (104)$$

However, it is more relevant to take for v_{max} the *exact* value (79), i.e.

$$v_{max} = \sqrt{2T \ln \left[\cosh \left(\frac{u}{T} \right) \right] - u^2}. \quad (105)$$

Typically, Eq. (103) with (104) gives a better agreement with the exact solution in the tail of profile while Eq. (103) with (105) gives a better agreement in the core of the profile, see Fig. 5. Finally, the surface tension calculated with Eq. (103) is given by $\sigma = \frac{4}{3}v_{max}^2L$.

3.7 Simple approximation for $T < 1/2$

For sufficiently small temperatures, we can propose a simple approximation of the wall profile in the form

$$\phi = u(T) \left[1 - e^{-2\tau/L(u)} \right] \quad (\tau \geq 0), \quad (106)$$

where u and L are given by the *exact* expressions (101) and (102). The concentration gradient obtained from Eq. (106) is

$$v(\tau) = v_{max}(T)e^{-2|\tau|/L(T)}, \quad (107)$$

with the maximum value $v_{max} = 2\frac{u}{L}$. As before, it may be more relevant to use the exact value (105). The surface tension calculated with Eq. (107) is given by $\sigma = \frac{1}{2}v_{max}^2L$ but this approximation yields, unfortunately, an asymptotic behaviour for $T \rightarrow 0$ different from the exact result (96).

The Ansatz (100)-(106) have a self-similar structure as a function of the temperature. Indeed, the functions $\phi(\tau)/u(T)$ and $v(\tau)/v_{max}(T)$ vs $\tau/L(T)$ have an invariant profile. The exact solution of the differential equation (66) has not an exact self-similar structure as shown in Figs. 10 and 11 but the region between the envelopes is relatively thin so that Eqs. (100)-(106) can be useful approximations for $T \rightarrow 1$ and $T \rightarrow 0$ respectively. The profiles of concentration and concentration gradient (in non-scaled variables) are plotted in Figs. 12 and 13.

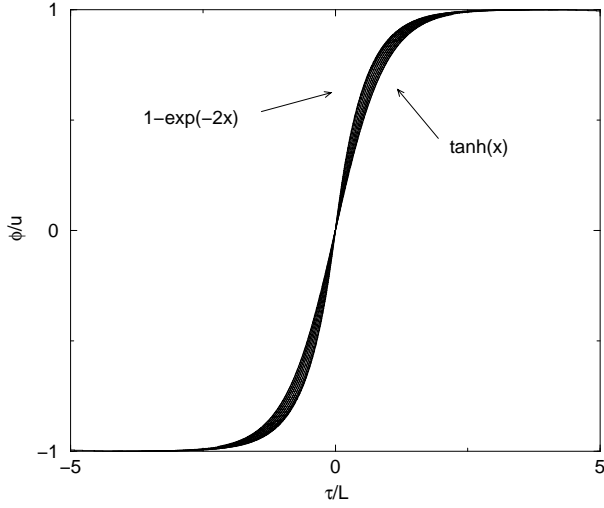


Fig. 10. Scaled concentration $\phi/u(T)$ as a function of the scaled distance $\tau/L(T)$ for different values of the temperature between $T = 0$ and $T = T_c = 1$. In terms of the scaled variables, the exact concentration profile is bounded by the solutions $1 - \exp(-2x)$ for $T = 0$ and $\tanh(x)$ for $T = T_c$.

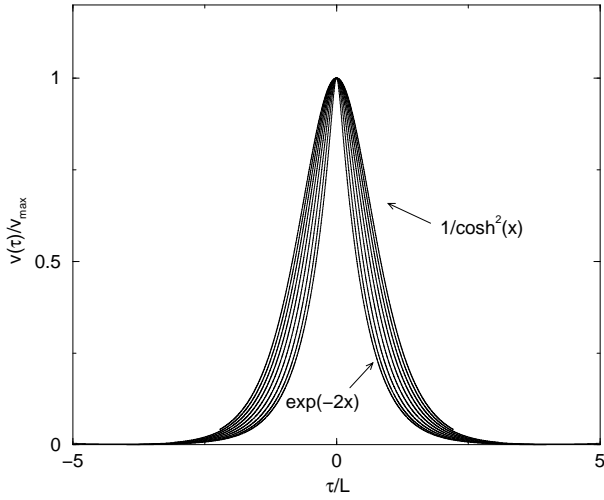


Fig. 11. Scaled concentration gradient $v/v_{max}(T)$ as a function of the scaled distance $\tau/L(T)$ for different values of the temperature between $T = 0$ and $T = T_c = 1$. In terms of the scaled variables, the exact profile of concentration gradient is bounded by the solutions $\exp(-2x)$ for $T = 0$ and $1/\cosh^2(x)$ for $T = T_c$.

3.8 Match asymptotics

For small values of the temperature, one can propose another approximation of the profiles of concentration and concentration gradient by using match asymptotics.

3.8.1 Concentration profile $\phi(\tau)$

The exact asymptotic behaviors of the concentration profile are given by

$$\phi(\tau) \simeq v_{max}\tau + \dots \quad (\tau \rightarrow 0), \quad (108)$$

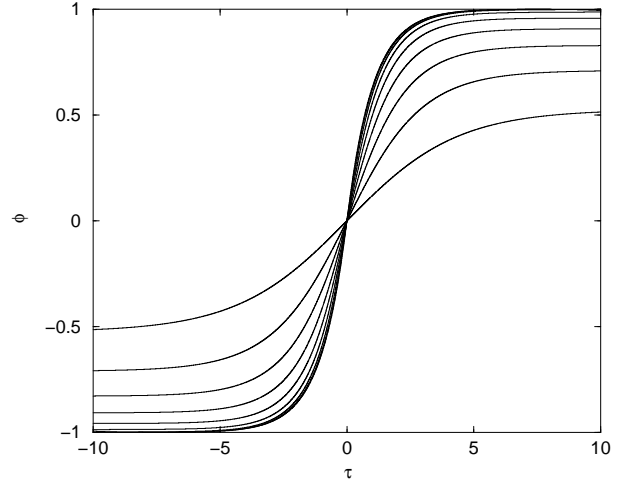


Fig. 12. Concentration ϕ as a function of the distance τ for different values of the temperature $T = 0.1, 0.2, 0.3, 0.4, 0.5, 0.6, 0.7, 0.8$ and 0.9 .

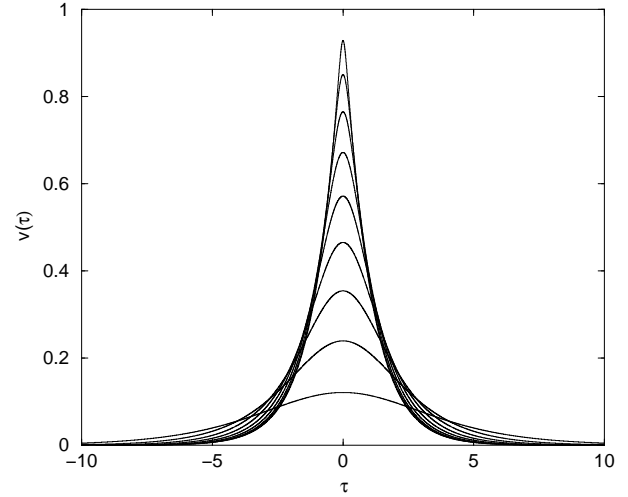


Fig. 13. Concentration gradient v as a function of the distance τ for different values of the temperature $T = 0.1, 0.2, 0.3, 0.4, 0.5, 0.6, 0.7, 0.8$ and 0.9 .

$$\phi(\tau) = u - Ae^{-2\tau/L} \quad (\tau \rightarrow +\infty), \quad (109)$$

where u , L and v_{max} are known functions of the temperature. We match these two behaviors at a point x where their values and the values of their first derivative coincide. This yields

$$x v_{max} = u - Ae^{-2x/L}, \quad (110)$$

$$v_{max} = \frac{2A}{L} e^{-2x/L}. \quad (111)$$

From these relations, we obtain

$$x = \frac{u}{v_{max}} - \frac{L}{2}, \quad (112)$$

$$A = \frac{L}{2} v_{max} e^{\frac{2u}{Lv_{max}} - 1}. \quad (113)$$

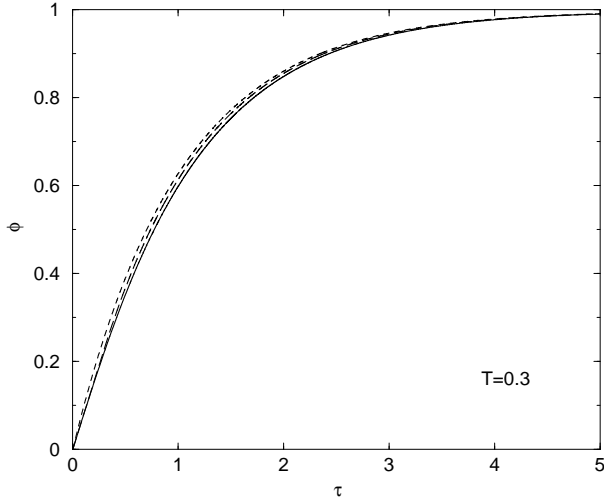


Fig. 14. Concentration profile for $T = 0.3$: exact (solid), approximate self-similar (dotted), match asymptotics (long-dashed).

For $T \rightarrow 0$, we explicitly find that

$$x = (\ln 2)T, \quad (114)$$

$$A = 1 - (\ln 2)^2 T^2. \quad (115)$$

The exact concentration profile is plotted in Fig. 14 for $T = 0.3$, and compared with the approximate self-similar expression (106) and the expression (108)-(109) obtained by match asymptotics.

3.8.2 Concentration gradient $v(\tau)$

The exact asymptotic behaviors of the concentration gradient are given by

$$v(\tau) \simeq v_{max} \left[1 + \frac{1}{2} \left(1 - \frac{1}{T} \right) \tau^2 + \dots \right] \quad (\tau \rightarrow 0), \quad (116)$$

$$v(\tau) = 2 \frac{A}{L} e^{-2\tau/L} \quad (\tau \rightarrow +\infty). \quad (117)$$

We match these two behaviors at a point x where their values and the values of their first derivative coincide. After simplification, we obtain

$$x = \frac{-L + \sqrt{L^2 + \frac{8T}{1-T}}}{2}, \quad (118)$$

$$A = \frac{L^2}{4} v_{max} \left(\frac{1}{T} - 1 \right) x e^{2x/L}. \quad (119)$$

For $T \rightarrow 0$, we explicitly find that

$$x = T, \quad (120)$$

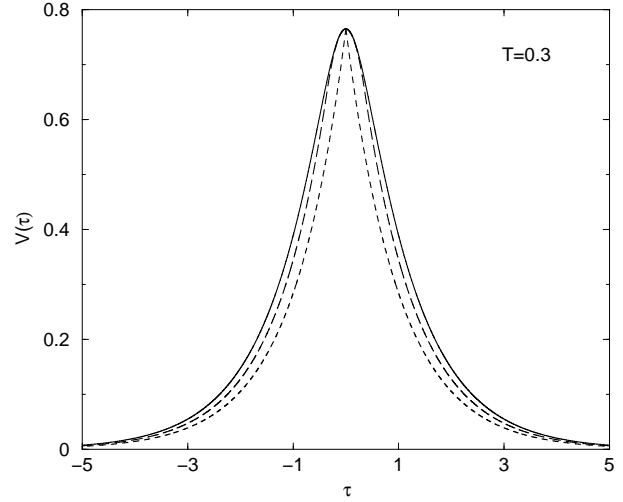


Fig. 15. Concentration gradient for $T = 0.3$: exact (solid), approximate self-similar (dotted), match asymptotics (long-dashed).

$$A = 1 + (1 - \ln 2)T. \quad (121)$$

The exact concentration gradient is plotted in Fig. 15 for $T = 0.3$, and compared with the approximate self-similar expression (107)-(105) and the expression (116)-(117) obtained by match asymptotics.

3.9 The curvature radius

To next order in the expansion in $k^{-1} \ll 1$, we must account for the curvature of the interface. Close to the interface, $\nabla\psi = \frac{d\psi}{d\xi} \mathbf{n}$ where \mathbf{n} is a unit vector normal to the wall. Introducing the curvature $r^{-1} = \nabla \cdot \mathbf{n}$ (r is the curvature radius), we get $\Delta\psi = d^2\psi/d\xi^2 + r^{-1}d\psi/d\xi$. Therefore, Eq. (56) becomes at first order

$$\frac{d^2\phi}{d\tau^2} + \frac{1}{kr} \frac{d\phi}{d\tau} = -U'(\phi) + \chi_1/k, \quad (122)$$

where we have written $\chi = \chi_0 + k^{-1}\chi_1 + \dots$ and used the fact that $\chi_0 = 0$ at leading order (see Sec. 3.3). Multiplying Eq. (122) by $d\phi/d\tau$ and integrating along the wall we obtain the relation

$$\frac{1}{r} = -\frac{2\chi_1 u}{\sigma(u)}, \quad (123)$$

which shows that the radius of curvature r is constant. Therefore, the shape of the interface is either a circle (leading to a spot) or a straight line (leading to a stripe). Equation (123) is similar to Laplace's law relating the curvature radius of bubbles to the surface tension and to the difference of pressure between the interface.

3.10 The free energy

The previous results can be recovered by minimizing the 'free energy' (21)-(22). This has been discussed by Bouchet

& Sommeria [24] in the context of jovian vortices where the problem is similar (see Sec. 4). Therefore, their study can be directly applied to the present situation and we shall only give the main steps of the analysis.

To leading order in $k^{-1} \rightarrow 0$, the system consists of two phases with uniform density $\rho_{\pm 1}$ and size $A_{\pm 1}$ (we call $A = A_+ + A_-$ the total size of the domain). Setting $\rho = \frac{\sigma_0}{2}(1 + \phi)$ and $c = \frac{\lambda\sigma_0}{2k^2}(1 + \phi)$, the free energy $F = E - T_{eff}S + \alpha T_{eff}M$ where E and S are given by Eqs. (21)-(22) and M is the total mass can be written

$$F = A_1 f(\rho_1) + (A - A_1) f(\rho_{-1}), \quad (124)$$

with

$$f = \frac{T_{eff}\sigma_0}{2} [-C\phi^2 + (\alpha - 2C)\phi + (1 + \phi)\ln(1 + \phi) + (1 - \phi)\ln(1 - \phi)]. \quad (125)$$

The optimal values of $\rho_{\pm 1}$ and $A_{\pm 1}$ are obtained by minimizing the free energy (124). The variations on $\rho_{\pm 1}$ imply that

$$f'(\rho_{\pm 1}) = 0, \quad f''(\rho_{\pm 1}) > 0. \quad (126)$$

and the variations on A_1 imply that

$$f(\rho_1) = f(\rho_{-1}). \quad (127)$$

This relation expresses the equality of the free energy of the two phases. The only possibility to satisfy the relations (126)-(127) simultaneously is to have $\alpha = 2C$ so that $f(\phi)$ is an odd function. This is equivalent to the solvability condition (65) leading to $\chi \equiv \alpha/2C - 1 = 0$. Then, it is straightforward to check that $f'(\rho) = 0$ implies that $\phi = \pm u$ where u is given by

$$Cu = \frac{1}{2} \ln \left(\frac{1+u}{1-u} \right) = \tanh^{-1}(u). \quad (128)$$

This returns the relation (68)-b.

To first order in k^{-1} , we need to determine the contribution of the free energy contained in the wall (interface). The free energy per unit length is given by

$$F_W = \frac{1}{k} \int_{-\infty}^{+\infty} [h(\rho(\tau)) - h(\rho_{\pm 1})] d\tau, \quad (129)$$

where $h(\rho)$ is the density of free energy. Using Eqs. (21), (22), (71) and (73), we obtain after simplification

$$F_W = \frac{\lambda\sigma_0^2}{4k^3} \int_{-\infty}^{+\infty} [\tilde{h}(\phi) - \tilde{h}(\phi_{\pm 1})] d\tau, \quad (130)$$

with

$$\tilde{h}(\phi) = \phi(\tanh(C\phi) - \phi). \quad (131)$$

Using $\tilde{h}(\phi_{\pm 1}) = \tilde{h}(u) = 0$ and $\tanh(C\phi) \geq \phi$ (see Fig. 1), we find that $F_W > 0$. Therefore, minimizing the free energy amounts to minimizing the length of the interface at fixed area. This gives either a circle or a straight line and

this returns the fact that the curvature radius is constant (see Sec. 3.9). This argument also shows that it is more profitable to form, at equilibrium, a single ‘‘bubble’’ of size A rather than several ‘‘droplets’’ of smaller size. However, a configuration with several ‘‘droplets’’ can exist as a non-equilibrium solution of the regularized Keller-Segel model (18)-(19). These droplets will evolve in time and merge together to finally form a single ‘‘bubble’’ (spot or stripe). This is similar to a coarsening process in spin systems or to the aggregation of vortices in 2D decaying turbulence [28].

3.11 Bifurcations: spots and stripes

We shall work in a square domain with total size A . We consider periodic boundary conditions in order to avoid boundary effects. The equilibrium state consists in two phases with uniform density (ρ_+, A_+) and (ρ_-, A_-) with $A_+ + A_- = A$. We introduce the parameter

$$B = 1 - \frac{2M}{\sigma_0 A}. \quad (132)$$

Since $0 \leq M \leq \sigma_0 A$, the parameter B takes values between -1 and $+1$. Writing $M = A_+ \rho_+ + A_- \rho_-$ and using Eq. (70), the area of the two phases at equilibrium are given by

$$A_{\pm} = \frac{A}{2} \left(1 \mp \frac{B}{u} \right). \quad (133)$$

They are determined by the parameter B (fixed by the total mass) and by the parameter u (fixed by the temperature). Since $0 \leq A_{\pm} \leq A$, we have the inequalities

$$|B| \leq u \leq 1, \quad -1 \leq B \leq 1. \quad (134)$$

Since the curvature radius is constant, we have three possible configurations: (i) a circular domain (spot) of phase $+$ surrounded by phase $-$: the length of the interface is $2\sqrt{\pi A_+}$. (ii) a circular domain (spot) of phase $-$ surrounded by phase $+$: in that case, the length of the interface is $2\sqrt{\pi(A - A_+)}$. (iii) a stripe of phase \pm and a stripe of phase \mp : the length of the interface is $2\sqrt{A}$. The configuration selected at equilibrium is the one with the smallest interfacial length (see Fig. 16).

(i) The spot of phase $+$ surrounded by phase $-$ will be selected if $A_+ \leq A/\pi$, i.e. $u \leq \pi B/(\pi - 2)$. This is possible only for $B \geq 0$. In terms of the temperature, this corresponds to $T \geq T_0$ where $T_0(B)$ is determined by $u_0 = \tanh(u_0/T_0)$ with $u_0 = |B|\pi/(\pi - 2)$.

(ii) The circular domain of phase $-$ surrounded by phase $+$ will be selected if $A_+ \geq (1 - 1/\pi)A$, i.e. $u \leq -\pi B/(\pi - 2)$. This is possible only for $B \leq 0$. In terms of the temperature, this corresponds to $T \geq T_0$.

(iii) The stripes will be selected for $T < T_0$. This is possible only for $|B| \leq B_c \equiv (\pi - 2)/\pi$ (i.e. $u_0 \leq 1$). For $B > 0$, the stripe $+$ has the smallest area ($A_+ \leq A_-$) and this is the opposite for $B < 0$.

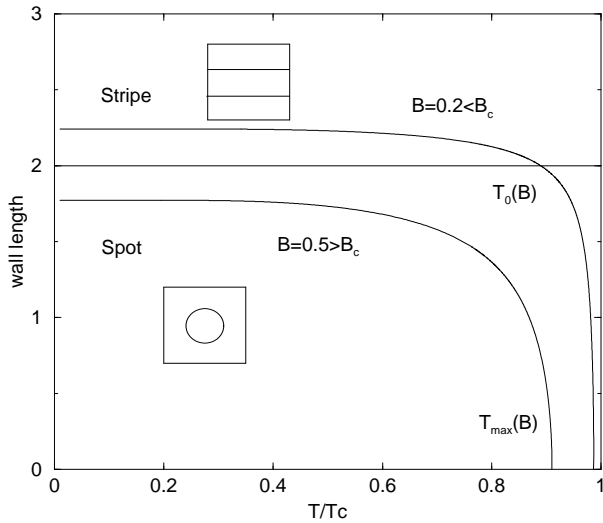


Fig. 16. Interfacial length of the spot (circle) as a function of the temperature for different values of the parameter B (the area of the domain has been normalized to $A = 1$). The spot is selected if its length is smaller than 2 and the stripe is selected in the other case. If $B > B_c = (\pi - 2)/\pi$, the spot is always selected. If $B < B_c$, the stripe is selected for $T < T_0(B)$ and the spot is selected for $T > T_0(B)$.

Finally, we note that the condition $|B| \leq u$ implies that $T \leq T_{max}(B) \leq T_c$ where $T_{max}(B)$ is determined by $|B| = \tanh(|B|/T_{max})$.

The phase diagram is represented in Fig. 17. This is the counterpart to the diagram obtained by Bouchet & Sommeria [24] for jovian vortices. The ‘spots’ are the equivalent of the ‘vortices’ and the ‘stripes’ are the equivalent of the ‘jets’. The main difference (beyond the context and the interpretation of the solutions) is that the control parameter in our case is the effective temperature T (“canonical” situation) while their control parameter is the energy E (microcanonical situation).

Finally, concerning the domain of validity, our approach assumes that the domain size is larger than the interfacial width $L(u)/k$ given by (77) so that $A_{\pm} \geq (2L/k)^2$. This is satisfied on the left of the dashed line in Fig. 17 corresponding to

$$|B| \leq u \left(1 - \frac{8L(u)^2}{Ak^2} \right). \quad (135)$$

4 Analogy with Jupiter’s great red spot

4.1 The physical context

Jupiter’s Great Red Spot (GRS) is probably the most famous example of vortex structures found in planetary atmospheres. The presence of this spot was first reported by Robert Hooke in 1664 in the first issue of the Philosophical Transaction of the Royal Society. The GRS is a large “eye” that dominates the southern hemisphere of the planet. It is an oval-shaped anticyclone with size

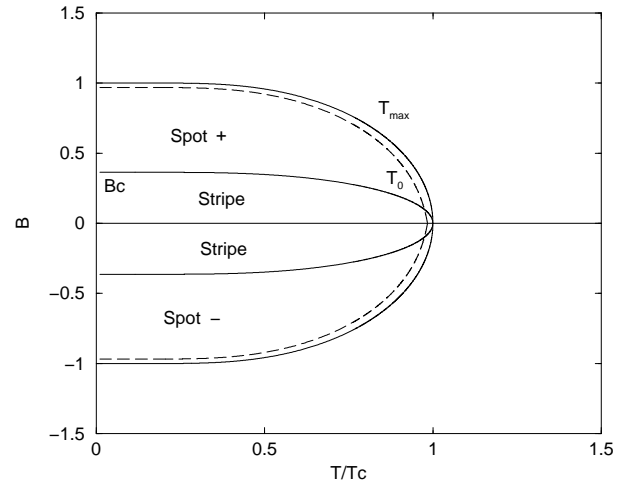


Fig. 17. Phase diagram of the regularized chemotactic model (18)-(19) showing the bifurcation between ‘spots’ and ‘stripes’ as a function of the control parameters (B, T) . In a bounded domain, the solutions exist only for $T \leq T_{max}(B)$. We have drawn the line of transition $T_0(B)$ between the two structures. Finally, the dashed line corresponds to the domain of validity of our perturbative expansion; it has been plotted for $Ak^2 = 1000$.

26000km by 13000km. Its breadth is about one hundred times its height so it can be considered approximately two-dimensional. It resides in a zonal shear at latitude 23S where the velocity changes sign, is elongated along the shear zone and is of the same sign as the background shear (these are relatively general rules observed for other vortices). It stays at the same latitude but slowly drifts in longitude. Morphologically, the GRS has a striking annular structure with a quiet center surrounded by a thin intense jet. The concentration of winds in an annulus is consistent with the fact that the GRS is much larger than the atmosphere’s radius of deformation (the jet’s width scales with the Rossby radius of deformation).

Some authors have tried to describe this spot as a soliton solution of a modified KdV equation but this interpretation as a weakly nonlinear structure faces several drawbacks: the jet structure is not reproduced and the soliton theory predicts an interpenetration without change of structure while the main interaction between vortices is a merging process. In contrast, Marcus [29] argues that a permanent vortex can coexist with turbulence and that most of the properties of the Jovian vortices can be easily explained and understood with the quasi-geostrophic (QG) theory. In addition, he emphasizes the jet structure of the GRS and shows that an annular jet is the natural structure of a vortex with a uniform potential vorticity inside and outside the spot. A physical justification of this construction was given by Sommeria et al. [23] in terms of statistical mechanics. A statistical theory of 2D turbulence has been developed by Miller [19] and Robert & Sommeria [20] following and generalizing the pioneering work of Onsager [30] on point vortices. This theory is able to account for the typical vortices (monopoles, dipoles, tripoles,...) observed in two-dimensional flows [31]. In the

QG model, and in the limit of small Rossby radius, PV mixing (entropic effects) with constraints on the energy leads to an equilibrium state that consists of two phases with uniform PV in contact separated by a strong jet. This precisely account for the morphology of the GRS. This model has been further developed by Bouchet & Sommeria [24] with quantitative applications to Jovian vortices. Another model has been proposed by Turkington et al. [32]. It predicts the emergence of a vortex solution at the correct latitude but it does not reproduce the annular jet structure of the GRS [33].

4.2 Statistical mechanics of the quasi-geostrophic equations

The quasi-geostrophic equations appropriate to the dynamics of geophysical flows [22] can be written:

$$\frac{\partial q}{\partial t} + \mathbf{u} \cdot \nabla q = 0, \quad (136)$$

$$q = -\Delta\psi + \frac{\psi}{R^2} - Rh(y), \quad \mathbf{u} = -\hat{\mathbf{z}} \times \nabla\psi. \quad (137)$$

Here, q is the potential vorticity (PV) and ψ the stream function ($\hat{\mathbf{z}}$ is a unit vector normal to the two-dimensional flow). We have assumed that the topography $Rh(y)$ scales with the Rossby radius R . The Q.G. equations admit an infinite number of stationary solutions specified by any relationship $q = f(\psi)$. For given initial conditions, the statistical theory selects the most probable state consistent with the constraints imposed by the dynamics. It is obtained by maximizing a mixing entropy at fixed energy and Casimir constraints [19, 20, 21].

Let us consider the situation where the fine-grained PV q takes only two values $\{a_{-1}, a_1\}$. It is convenient to set $(a_1 - a_{-1})/2 = 1$ and $(a_1 + a_{-1})/2 = B$. We also choose the Gauge condition on ψ such that $\langle q \rangle = 0$ [24]. Then, the total area occupied by level a_1 is $\mathcal{A} = (1 - B)/2$ (the total area of the domain is unity). In this two-levels case [19, 20, 21], the mixing entropy is given by

$$S = - \int [p \ln p + (1 - p) \ln(1 - p)] d\mathbf{r}, \quad (138)$$

where $p(\mathbf{r})$ is the local distribution of level a_1 . The coarse-grained PV is $\bar{q} = pa_1 + (1 - p)a_{-1}$. The extremization of (138) at fixed energy

$$E = \frac{1}{2} \int (\bar{q} + h)\psi d\mathbf{r} = \frac{1}{2} \int [(\nabla\psi)^2 + \frac{\psi^2}{R^2}] d\mathbf{r}, \quad (139)$$

and total area $\mathcal{A} = \int p(\mathbf{r}) d\mathbf{r}$ leads to a $q - \psi$ relation of the form

$$\bar{q} = B - \tanh\left(\alpha - \frac{C\psi}{R^2}\right), \quad (140)$$

where α and C are Lagrange multipliers introduced in the variational problem $\delta S - 2\alpha\delta\mathcal{A} + \frac{C}{R^2}\delta E = 0$.

Robert & Sommeria [34] have proposed a parameterization of 2D turbulence in the form of a relaxation equation for the coarse-grained PV $\bar{q}(\mathbf{r}, t)$. This parameterization is based on a Maximum Entropy Production Principle (MEPP). The diffusion current (due to turbulent mixing) is assumed to maximize the rate of entropy production \dot{S} while conserving all the constraints imposed by the dynamics. In the two-levels case, this yields a system of equations of the form

$$\frac{\partial \bar{q}}{\partial t} + \mathbf{u} \cdot \nabla \bar{q} = \nabla \cdot [D(\nabla \bar{q} + \beta(t)(a_1 - \bar{q})(\bar{q} - a_{-1})\nabla\psi)], \quad (141)$$

$$\beta(t) = - \frac{\int D \nabla \bar{q} \cdot \nabla \psi d\mathbf{r}}{\int D(a_1 - \bar{q})(\bar{q} - a_{-1})(\nabla\psi)^2 d\mathbf{r}}, \quad (142)$$

$$q = -\Delta\psi + \frac{\psi}{R^2} - Rh(y). \quad (143)$$

Interestingly, these drift-diffusion equations are similar to the regularized chemotactic model (18)-(19). In this analogy, the coarse-grained PV \bar{q} plays the role of the bacterial concentration and the stream function ψ the role of the chemical c . This analogy was noted in [4]. An important difference, however, is that in 2D turbulence the energy is conserved so that the inverse temperature $\beta(t)$ evolves in time. By contrast, in the chemotactic problem, we are in a situation where the ‘effective temperature’ $T_{eff} = 1/\beta$ is fixed. Therefore, 2D turbulence corresponds to a micro-canonical situation (where we maximize the entropy S at fixed energy E) while chemotaxis corresponds to a canonical situation (where we minimize an effective free energy $F = E - T_{eff}S$). These two situations are described in [15]. For long-range interactions ($k = 0$ or $R \rightarrow +\infty$), the ‘ensembles’ are generically inequivalent. However, in the limit that we consider here, corresponding to a short-range interaction, they become equivalent, i.e. the $\beta(E)$ curve is univalued (see Fig. 18).

The equilibrium problem (140)-(143) has been studied in the limit of small Rossby radius $R \rightarrow 0$. The original idea dates back to Sommeria et al. [23] who understood that, in this limit, the solution is made of two uniform PV regions separated by a strong jet. This model has been developed quantitatively by Bouchet & Sommeria [24] with comparison to jovian data. Our study of the regularized chemotactic problem has been directly inspired by these works. In complement, we have provided in Sec. 3 a more thorough study of the wall equation with useful asymptotic expansions and analytical approximations. Due to the analogy between the two problems, these results can also be relevant to describe the jet structure of jovian vortices, like GRS. In this respect, we recall that the GRS corresponds to a typical parameter u in the range $0.92 \leq u \leq 1$ [24] so that the limit $u \rightarrow 1$ or $T \rightarrow 0$ of our study (Secs. 3.5, 3.7 and 3.8) is particularly interesting in that respect. To strengthen the comparison between the two problems (chemotaxis and jovian vortices), we briefly recall the main lines of the study of Bouchet & Sommeria [24] and provide some complementary discussion.

4.3 Domain wall theory of Jupiter's great red spot

4.3.1 The jet equation

Combining Eqs. (143) and (140), we find that the streamfunction satisfies the meanfield equation

$$-\Delta\psi + \frac{\psi}{R^2} - Rh(y) = B - \tanh\left(\alpha - \frac{C\psi}{R^2}\right). \quad (144)$$

We shall solve this equation perturbatively as an expansion in powers of R . We only give the main lines and refer to Bouchet & Sommeria [24] for more details and developments. To first order, we obtain the jet equation

$$-\frac{d^2\psi}{d\xi^2} - \frac{1}{r}\frac{d\psi}{d\xi} + \frac{\psi}{R^2} - Rh(y) = B - \tanh\left(\alpha - \frac{C\psi}{R^2}\right), \quad (145)$$

where r is the curvature radius. Introducing the notations

$$\tau = \xi/R, \quad \phi = \frac{\psi}{R^2} - \frac{\alpha}{C}, \quad (146)$$

we get

$$\frac{d^2\phi}{d\tau^2} + \frac{R}{r}\frac{d\phi}{d\tau} + Rh(y) = -\tanh(C\phi) + \phi + \frac{\alpha}{C} - B. \quad (147)$$

To leading order in $R \ll 1$, the foregoing equation reduces to

$$\frac{d^2\phi}{d\tau^2} = -\tanh(C\phi) + \phi + \frac{\alpha_0}{C} - B. \quad (148)$$

The condition of solvability implies that $\alpha_0 = CB$ so that the jet equation takes the form

$$\frac{d^2\phi}{d\tau^2} = -\tanh(C\phi) + \phi = -U'(\phi). \quad (149)$$

This is the same equation as Eq. (66) with $C = 1/T$. In the present context, ϕ is related to the streamfunction and $v = d\phi/d\tau$ to the jet velocity. Therefore, the figures representing the profile of concentration gradient in Sec. 3 give the jet velocity profile in the present context. The PV and streamfunction in the two phases are

$$q_{\pm} = \frac{\psi_{\pm}}{R^2} = B \pm u. \quad (150)$$

Their area is given by

$$A_{\pm} = \frac{1}{2} \left(1 \mp \frac{B}{u} \right), \quad (151)$$

which is similar to Eq. (133). Finally, in the present context, the parameter u is determined by the energy according to the relation

$$E = \frac{1}{2} R^2 (u^2 - B^2). \quad (152)$$

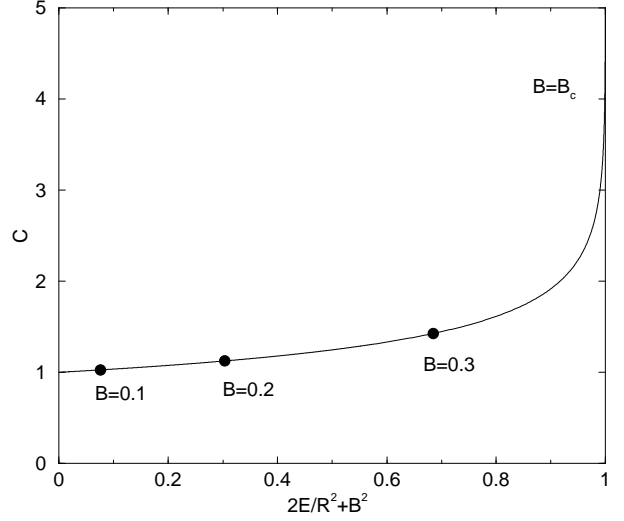


Fig. 18. Caloric curve giving the inverse temperature C as a function of the energy E for jovian vortices in the limit of small radius of deformation $R \rightarrow 0$. This curve is obtained from Eq. (152)-(68) in the absence of topography. In terms of the variable $2E/R^2 + B^2$, this curve is independent on B . We have indicated by a ‘bullet’ the point of bifurcation (corresponding to $u = \pi B/(\pi - 2)$) between a vortex (spot, left) and a straight jet (stripe, left), for different values of B : 0.1, 0.2 and 0.3.

4.3.2 The underlying shear

To first order in R , the jet equation can be written

$$\frac{d^2\phi}{d\tau^2} + \frac{R}{r}\frac{d\phi}{d\tau} + Rh(y) = -U'(\phi) + R\alpha_1, \quad (153)$$

where we have written $\alpha = \alpha_0 + R\alpha_1 + \dots$ and used $\alpha_0 = CB$. Far from the jet, we have

$$Rh(y) = -U'(\phi) + R\alpha_1. \quad (154)$$

Writing $\phi = u + R\delta\phi$, we get $\delta\phi = (\alpha_1 - h(y))/U''(u)$ so that the velocity $\mathbf{v}_{shear} = \delta\phi'(y)\mathbf{e}_x$ is given by

$$v_{shear} = \frac{h'(y)}{-U''(u)} = \frac{h'(y)}{1 - C(1 - u^2)}. \quad (155)$$

Now, the analysis of the jet equation in Sec. 3.3 shows that the function appearing in the denominator of Eq. (155) is related to the jet width (77) so that we can write

$$v_{shear}(y) = \frac{1}{4} h'(y) L(u)^2. \quad (156)$$

4.3.3 The curvature-topography relation

Finally, multiplying Eq. (153) by $d\phi/d\tau$ and integrating across the jet, we obtain

$$\frac{e(u)}{r} = u(h(y) - \alpha_1), \quad (157)$$

which relates the radius of curvature r to the underlying topography $h(y)$. For a given topography, Eq. (157) determines the form of the jet. This problem has been studied in detail in Bouchet & Sommeria [24] in the case of a quadratic topography. As another example, we consider here the inverse problem: given the form of the jet, find the corresponding topography. We consider the case of an elliptical vortex (see Fig. 19) because this is a relatively good representation of Jupiter's great red spot and we can obtain analytical results in that case.

The topography leading to an elliptic vortex has the form

$$h(y) = \frac{H}{\left[1 + (y/L)^2\right]^{3/2}}, \quad (158)$$

where L and H are typical horizontal and vertical length scales. Assuming that this relation holds for $|y| \rightarrow +\infty$, we must take $\alpha_1 = 0$ in Eq. (157) to have a vanishing curvature at infinity where $h \rightarrow 0$. Therefore, the curvature radius of the vortex is given by

$$\frac{L\chi}{r} = \left[1 + (y/L)^2\right]^{-3/2}, \quad (159)$$

where we have defined $\chi = e(u)/uHL$. This is the equation of an ellipse with major and minor semi-axis:

$$a = \frac{L\chi}{1 - \chi^2}, \quad b = \frac{L\chi}{\sqrt{1 - \chi^2}}. \quad (160)$$

These relations assume that $\chi \leq 1$. Now, in the case of GRS, the aspect ratio

$$\frac{a}{b} = \frac{1}{\sqrt{1 - \chi^2}}, \quad (161)$$

is close to 2 leading to $\chi = \sqrt{3}/2$. The major and minor semi-axis are then given by $a = 2\sqrt{3}L$ and $b = \sqrt{3}L$.

Consider now the limit $\chi \rightarrow 0$. In that case, the width of the vortex is small with respect to the horizontal topographic length ($b \ll L$) and we can make the quadratic approximation

$$h(y) \simeq H - \frac{3}{2} \frac{H}{L^2} y^2. \quad (162)$$

This is similar to the situation considered by Bouchet & Sommeria [24]. Their parameter d is related to our parameter χ by $d = (3/2)\chi^2$. For a quadratic topography with $(\chi, d) \rightarrow 0$, our study shows that the vortex shape is an ellipse whose major and minor semi-axis are given by Eqs. (160). In particular, the aspect ratio behaves like

$$\frac{a}{b} = 1 + \frac{d}{3} + \dots \quad (d \rightarrow 0). \quad (163)$$

This formula is not applicable for a vortex with aspect ratio ~ 2 like GRS. Bouchet & Sommeria [24] assume a quadratic topography and solve the curvature-topography

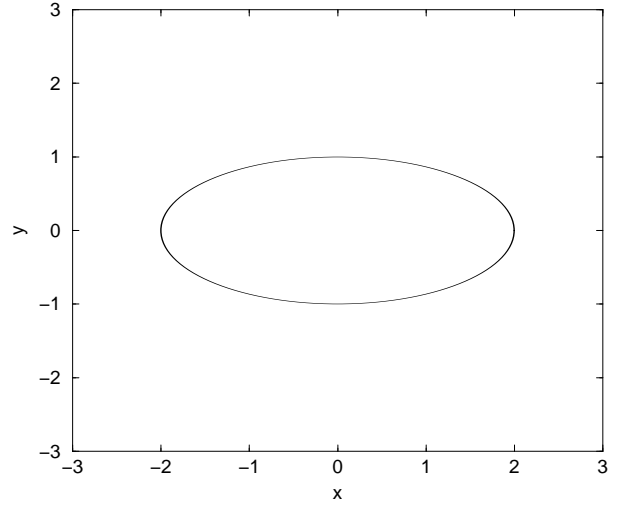


Fig. 19. Elliptic vortex with aspect ratio of 2 above a topography of the form (158).

relation numerically. For large values of d , close to its maximal value $d_{max} = 4/9$, the vortex is not an ellipse. Alternatively, if we assume a topography of the form (158) we find an elliptic vortex for all the values of $\chi \leq 1$. Therefore, the form of the vortex is relatively sensitive to the underlying topography.

5 Conclusion

In this paper, we have studied the equilibrium states of a regularized version of the Keller-Segel model describing the chemotactic aggregation of bacterial colonies. The regularization is justified physically in order to avoid the formation of singularities (Dirac peaks) during the dynamics and obtain smooth density profiles (clumps) instead. This regularization accounts for finite size effects and close packing effects. In that case, an equilibrium state exists for any value of the control parameter (this is similar to considering a gas of self-gravitating fermions in astrophysics to avoid complete gravitational collapse [35]). We have studied furthermore a limit of high degradation $k \rightarrow +\infty$. In previous works [5, 6, 7, 8, 9, 10, 11, 12], the opposite limit $k = 0$ (no degradation) was considered instead. The intermediate case of a finite degradation must be studied numerically (in preparation). However, the asymptotic limit $k \rightarrow +\infty$ allows us to obtain analytical results that permit to have a clear picture of the bifurcation diagram (between spots and stripes) in parameter space. Furthermore, our approach is exact in one dimension, for any value of the degradation rate k . Our study shows that the physics of the problem is sensibly different whether $k = 0$ or $k \neq 0$.

We have also discussed the analogy between the organization of bacteria (in stripes and spots) in the chemotactic problem and the organization of two-dimensional turbulent flows (in jets and vortices) in the jovian atmosphere. These apparently completely different systems are however described by relatively similar equations so that

an interesting analogy can be developed between the two. In this analogy, the jet structure of Jupiter's great red spot can be seen as a 'domain wall' that is similar to the interface separating two phases in contact, as in the biological problem.

A Stability analysis

We study the linear dynamical stability of an infinite and homogeneous solution of the regularized Keller-Segel model (18)-(19). The unperturbed solution is such that

$$k^2 c = \lambda \rho. \quad (164)$$

Linearizing Eqs. (18)-(19) around this steady state and writing the perturbation as $\delta \rho = \delta \hat{\rho} e^{i\mathbf{q}\cdot\mathbf{r}} e^{\sigma t}$, $\delta c = \delta \hat{c} e^{i\mathbf{q}\cdot\mathbf{r}} e^{\sigma t}$, we obtain

$$\chi \rho (1 - \rho/\sigma_0) q^2 \delta \hat{c} - (Dq^2 + \sigma) \delta \hat{\rho} = 0, \quad (165)$$

$$(q^2 + k^2) \delta \hat{c} - \lambda \delta \hat{\rho} = 0. \quad (166)$$

This system of equations admits non-trivial solutions only if the determinant is zero yielding the dispersion relation

$$\sigma = q^2 \left(\frac{\chi \lambda \rho (1 - \rho/\sigma_0)}{q^2 + k^2} - D \right). \quad (167)$$

The system is unstable if $\sigma > 0$ and stable otherwise. A necessary condition of instability is

$$\frac{\chi}{D} \lambda \rho (1 - \rho/\sigma_0) - k^2 \geq 0. \quad (168)$$

If this condition is fulfilled, the unstable wavenumbers are

$$q^2 \leq \frac{\chi}{D} \lambda \rho (1 - \rho/\sigma_0) - k^2 \equiv q_{max}^2. \quad (169)$$

For $u = 0$, i.e. $\rho = \sigma_0/2$, we find that the instability criterion (168) corresponds to

$$T \leq T_c = 1. \quad (170)$$

Therefore, the uniform phase $u = 0$ is stable for $T > T_c$ and unstable for $T < T_c$ where it is replaced by a 'stripe' or a 'spot' (see Fig. 2). The unstable wavenumbers are

$$q^2 \leq (C - 1)k^2 \equiv q_{max}^2, \quad (171)$$

where we recall that $C = 1/T$. The growth rate (see Fig. 20) can be written

$$\sigma = Dq^2 \left(\frac{Ck^2}{q^2 + k^2} - 1 \right). \quad (172)$$

The maximum growth rate is obtained for

$$q_*^2 = k^2(\sqrt{C} - 1), \quad (173)$$

and its value is

$$\sigma_* = Dk^2(\sqrt{C} - 1)^2. \quad (174)$$

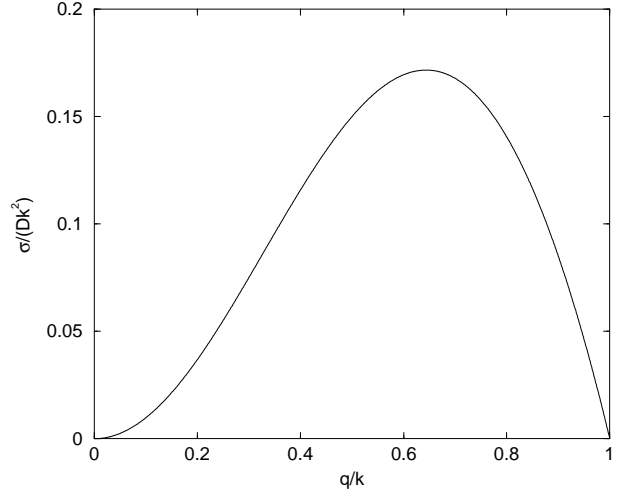


Fig. 20. Growth rate of the perturbation as a function of the wavenumber for $T = 1/2 < T_c$.

B Surface tension for $T \rightarrow 0$

Using Eqs. (80) and (72), the surface tension can be written

$$\sigma = 2 \int_0^u (\phi^2 - 2T \ln [\cosh(\phi/T)] - u^2 + 2T \ln [\cosh(u/T)])^{1/2} d\phi. \quad (175)$$

Using

$$\ln [\cosh(\phi/T)] = \phi/T - \ln 2 + \ln(1 + e^{-2\phi/T}), \quad (176)$$

and considering the limit $T \rightarrow 0$, we obtain

$$\sigma = 2 \int_0^1 \sqrt{(1 - \phi)^2 - 2T \ln(1 - e^{-2/T} + e^{-2\phi/T})} d\phi. \quad (177)$$

Setting $x = 1 - \phi$, this can be rewritten

$$\sigma = 2 \int_0^1 x \sqrt{1 - \frac{2T}{x^2} \ln [1 + e^{-2/T}(e^{2x/T} - 1)]} dx. \quad (178)$$

For $T \rightarrow 0$, we obtain

$$\sigma = 2 \int_0^1 x \left(1 - \frac{T}{x^2} \ln [1 + e^{-2/T}(e^{2x/T} - 1)] \right) dx. \quad (179)$$

Setting $y = 2x/T$, we find that

$$\sigma = 1 - 2T \int_0^{2/T} \ln [1 + e^{-2/T}(e^y - 1)] \frac{dy}{y}. \quad (180)$$

Setting $x = 2/T - y$, we get

$$\sigma = 1 - 2T \int_0^{2/T} \ln \left[1 + e^{-2/T} (e^{2/T-x} - 1) \right] \frac{dx}{2/T - x}. \quad (181)$$

For $T \rightarrow 0$, we finally obtain

$$\sigma = 1 - T^2 \int_0^{+\infty} \ln(1 + e^{-x}) dx. \quad (182)$$

Using

$$\int_0^{+\infty} \ln(1 + e^{-x}) dx = \frac{\pi^2}{12}, \quad (183)$$

we establish Eq. (96).

References

1. J.D. Murray, *Mathematical Biology* (Springer, Berlin, 1991)
2. C.S. Patlak, *Bull. of Math. Biophys.* **15**, 311 (1953)
3. E.F. Keller and L.A. Segel, *J. Theor. Biol.* **30**, 225 (1971)
4. P.H. Chavanis, M. Ribot, C. Rosier, C. Sire, *Banach Center Publ.* **66**, 103 (2004)
5. P.H. Chavanis, C. Rosier and C. Sire, *Phys. Rev. E* **66**, 036105 (2002).
6. C. Sire and P.H. Chavanis, *Phys. Rev. E* **66**, 046133 (2002).
7. P.H. Chavanis and C. Sire, *Phys. Rev. E* **69**, 016116 (2004).
8. C. Sire and P.H. Chavanis, *Phys. Rev. E* **69**, 066109 (2004).
9. P.H. Chavanis and C. Sire, *Phys. Rev. E* **70**, 026115 (2004).
10. C. Sire and P.H. Chavanis, *Banach Center Publ.* **66**, 287 (2004).
11. J. Sopik, C. Sire and P.H. Chavanis, *Phys. Rev. E* **72**, 026105 (2005).
12. P.H. Chavanis and C. Sire, [cond-mat/0504718]
13. D. Horstmann, *Jahresberichte der DMV* **106**, 51 (2004).
14. A. Bray, *Adv. Phys.* **43**, 357 (1994).
15. P.H. Chavanis, *Phys. Rev. E* **68**, 036108 (2003).
16. J. Sopik, C. Sire and P.H. Chavanis [cond-mat/0511347].
17. P.H. Chavanis, in *Dynamics and thermodynamics of systems with long range interactions*, edited by Dauxois, T., Ruffo, S., Arimondo, E. and Wilkens, M. *Lecture Notes in Physics*, Springer (2002); cond-mat/0212223
18. D. Lynden-Bell, *Mon. Not. Roy. Astr. Soc.* **136**, 101 (1967).
19. J. Miller, *Phys. Rev. Lett.* **65**, 2137 (1990).
20. R. Robert and J. Sommeria, *J. Fluid Mech.* **229**, 291 (1991).
21. P.H. Chavanis, J. Sommeria and R. Robert, *Astrophys. J.* **471**, 385 (1996).
22. J. Pedlosky, *Geophysical Fluid Dynamics* (Springer, Berlin, 1987)
23. J. Sommeria, C. Nore, T. Dumont and R. Robert, *C. R. Acad. Sci. Ser. II* **312**, 999 (1991).
24. F. Bouchet and J. Sommeria, *J. Fluid Mech.* **464**, 165 (2002).
25. W. Jäger, S. Luckhaus, *Trans. Amer. Math. Soc.* **329**, 819 (1992).
26. G. Kaniadakis, *Physica A* **296**, 405 (2001).
27. J.W. Cahn and J.E. Hilliard, *J. Chem. Phys.* **28**, 258 (1958).
28. C. Sire and P.H. Chavanis, *Phys. Rev. E* **61**, 6644 (2000).
29. P.S. Marcus, *Annu. Rev. Astron. Astrophys.* **31**, 523 (1993).
30. L. Onsager, *Nuovo Cimento Suppl.* **6**, 279 (1949).
31. P.H. Chavanis and J. Sommeria, *J. Fluid Mech* **356**, 259 (1998).
32. B. Turkington, A. Majda, K. Haven, M. Dibattista, *PNAS* **98**, 12346 (2001).
33. P.H. Chavanis, *Physica D* **200**, 257 (2005).
34. R. Robert and J. Sommeria, *Phys. Rev. Lett.* **69**, 2776 (1992).
35. P.H. Chavanis, *Phys. Rev. E* **65**, 056123 (2002).